Digital Control of PV Systems: Dynamic-Gain MPPT Algorithm and Effects of Resolution

Alon Blumenfeld and Mor Mordechai Peretz
Power Electronics Laboratory
Department of Electrical and Computer Engineering
Ben-Gurion University of the Negev
Beer-Sheva, Israel
alonblu@bgu.ac.il; morp@ee.bgu.ac.il
http://www.ee.bgu.ac.il/~pel

***Abstract*— This paper introduces a dynamic-gain MPPT algorithm for PV systems. The method demonstrates a rapid and uniform convergence toward the MPP by employing dynamic steps while owning MPPT control compatibility even for differential power processors. A theoretical analysis on the effects of resolution on limit cycle oscillations existence and power curve traps in the MPPT process is provided. The dynamic gain MPPT algorithm is demonstrated by simulation and experiments, avoiding limit cycle oscillations and power curve traps. The presented algorithm is verified on bi-directional differential power processors, demonstrating dynamic MPP convergence with no limit cycle oscillations and significant improvement of power harvesting capability up to 42%.**

I. INTRODUCTION

Tracking the maximum power point (MPP) of photovoltaic (PV) elements is of major concern in many solar energy harvesting systems. Recently, the realization of MPP tracking (MPPT) that is compatible for various mismatch conditions of the PV array has received increased attention [1]. Environmental conditions such as shading (full or partial), non-homogeneous dirt and defects result accelerate degradation of the PV element (PVE) [2], and as a consequence, alter the characteristics of the PVE, introducing two or more local power peaks rather that one global MPP. This requires modifications of the MPPT algorithm in order to obtain the maximum power out of a serially connected chain of PVEs. It should be noted however, that even though that the global MPPT is obtained, the extracted power out of the chain may fall below the maximum power available out of the chain [3].

Several solutions have been proposed and are widely covered in [3]. One of the more energy efficient solutions is the differential power processing (DPP) approach [4-8]. This concept applies processing only the power differences between PV elements, thus minimizes conversion losses and improves reliability. The differential processing can be obtained between the individual PVEs to a shared bus [4,5] or by creating active, local, PV-to-PV bypasses such as in [5-8]. The main challenge of present-day DPP-based architectures is the realization of MPPT algorithm on the individual units that is capable to converge to the local MPP of the individual PVE without affecting, or being affected by the operation of the neighboring PVEs. The DPP architecture and operation method in [8] describes a recently-developed resonant switched-capacitor gyrator converter (RSCGC) and a conceptual MPPT operation based on modification of the "hill climbing" MPPT (HC MPPT) method with variable-step variations. The method has demonstrated reliable operation, however, the convergence rate has been sacrificed to assure oscillation-free operation in the steady-state, around the MPP. Solutions to increase the convergence rate toward the MPP while assuring steady-state stability, were proposed using modifications of the "Perturb and Observe" (P&O) and the "hill climbing" methods implementing variable step size have been studied in [9, 10] on a centralized MPPT unit. Another interesting MPPT concept is the "incremental conductance" (IncCond) [11, 12], there the algorithm relies on the derivative of the instantaneous power with respect to the voltage, which reduces the mismatch effects and allows more accurate tracking of the MPP.

Most modern MPPT algorithms are realized using digital processing. As a result, issues related to digital control such as sampling resolutions of both current and voltage may introduce undesirable behavior. Power curve traps [13] and/or limit cycle oscillations (LCO) [14-16] may be of major concern for successful MPPT implementation.

The objective of this study is to present and explore a new MPPT method that hybrids a modified IncCond method with a dynamic step size operation. The new approach does not require continuous perturbations, it features fast dynamic performance as well as accurate static characteristics for a wide range of insolation levels, and is well suited for the use in both centralized or local (i.e. DPP) MPPT. This study further provides a detailed analysis on the effects of digital sampling resolutions that may cause power curve traps and steady-state LCO.

II. NORMALIZED INCREMENTAL CONDUCTANCE MPPT ALGORITHM

The precursors of the MPPT method developed are the variable gain HC MPPT of [9] and the IncCond method [11]. In this modification, the method applies a combined normalization of the PV power curve based on both the current and voltage, depending on the specific region of the power curve, i.e. below or above the MPP. Fig. 1 illustrates typical power curves for various insolation levels, as can be observed, the *p*-*v* and *p*-*i* relations result in locally concaved functions where the MPP is characterized by a zero gradient, at all insolation conditions.

978-1-4799-2147-8/14/$31.00 ©2014 IEEE

The aim of an MPPT algorithm is to converge into a zero gradient, i.e. $dp_{PV}/dv_{PV} \approx 0$ or $dp_{PV}/di_{PV} \approx 0$. As can be observed from Fig. 1, realization of the algorithm based on one of the power derivative (either current or voltage), results in a proportional, but asymmetrical derivative value for regions below and above the MPP [12]. To remedy this, a new derivative factor $e[n]$ that combines two power derivations, is defined by:

$$e[n] = \begin{cases} dp_{PV} / dv_{PV} & ; \quad v_{PV} \le V_{MPP} \\ -(dp_{PV} / di_{PV}) & ; \quad v_{PV} > V_{MPP} \end{cases}, \qquad (1)$$

where v_{PV} and V_{MPP} are the instantaneous and the MPP voltages of the PVE, respectively. By separation of the regions below and above V_{MPP}, the derivative factor $e[n]$ has a more symmetrical proportion with respect to the distance from V_{MPP}. It should be noted that merging dp_{PV}/dv_{PV} and dp_{PV}/di_{PV} still results in a smooth function without singularities.

Substituting $p_{PV} = v_{PV} \times i_{PV}$ in (1), and after some manipulations, (1) can be rewritten as:

$$e[n] = \begin{cases} i_{PV}[n] + \dfrac{di_{PV}}{dv_{PV}} v_{PV}[n] & ; \quad v \le V_{MPP} \\ -\left(v_{PV}[n] + \dfrac{dv_{PV}}{di_{PV}} i_{PV}[n] \right) & ; \quad v > V_{MPP} \end{cases}. \qquad (2)$$

where the index $[n]$ represents the n^{th} iteration of the algorithm.

The differential values of (2) can be realized by the controller as:

$$\begin{cases} dp_{PV} = p_{PV}[n] - p_{PV}[n-1] \\ dv_{PV} = v_{PV}[n] - v_{PV}[n-1] \\ di_{PV} = i_{PV}[n] - i_{PV}[n-1] \end{cases}, \qquad (3)$$

To expedite the convergence toward the MPP, variable step control is applied based on the value of $e[n]$. A correction signal $A[n]$ (e.g. duty ratio, dead-time, or frequency, depending on the converter topology) is generated according to an integral control law, as:

$$A[n] = A[n-1] + K_1 \times K_2[n] \times e[n], \qquad (4)$$

where K_1 is the magnitude constant coefficient, and $K_2[n]$ is the integral gain. To facilitate a generic control law for all insolation levels, the integral gain $K_2[n]$ is assigned as a dynamic normalizing factor as:

$$K_2[n] = \begin{cases} 1/i_{PV}[n] & ; \quad v \le V_{MPP} \\ 1/v_{PV}[n] & ; \quad v > V_{MPP} \end{cases}. \qquad (5)$$

Combining (2), (4) and (5) yields a new normalized error signal of the product $K_2 \times e[n]$, named dp_n, which can be expressed as:

$$dp_n = \begin{cases} 1 + \dfrac{di_{PV}}{dv_{PV}} \times \dfrac{v_{PV}[n]}{i_{PV}[n]} & ; \quad v \le V_{MPP} \\ -\left[1 + \left(\dfrac{di_{PV}}{dv_{PV}} \times \dfrac{v_{PV}[n]}{i_{PV}[n]} \right)^{-1} \right] & ; \quad v > V_{MPP} \end{cases}. \qquad (6)$$

The resultant dp_n is bounded within [-1, 1] as depicted in Fig. 1. By employing the normalized error, dp_n, the convergence to the MPP is uniform and not affected by the insolation conditions, while preserving proportional MPP value. To avoid the need of V_{MPP} for selecting the dp_n expression for the control, the smaller between the two possible dp_n values is selected. A detailed description of the algorithm is given by the flowchart of Fig. 2.

The convergence time of the MPPT algorithm and its pattern are primarily dependent on the magnitude constant K_1 that determines the step size of the control signal $A[n]$. For small correction steps the convergence would be smooth but slow, whereas large correction steps would result in rapid convergence but may introduce an oscillating error around the MPP. In this work, K_1 has been manually selected to produce the fastest convergence while still maintaining a first order pattern (i.e., without overshoot).

III. Resolution Effects on Limit Cycles

Convergence of any MPPT error signal (dp_n in this particular study) to zero is impractical due to the discrete-time nature of the control signal $A[n]$ (PWM generated by the DCO). Furthermore, the measured error signal is of a discrete nature as well. The resolution of the measured error signal and the generated control signal $A[n]$ has to be carefully selected to assure stability around MPP, i.e. to avoid limit cycle oscillations [14].

A. Theoretical LCO criterion

A key criterion for determining the existence of limit-cycle oscillations in digitally controlled MPPT system relies on the comparison between two main variables. The first is the smallest measurable sensed error signal Δ_r, (i.e., resolution) and the error signal variation due to a LSB change in $A[n]$ [12-14], Δ_e. Namely, a necessary condition for no LCO is that Δ_e, is smaller than Δ_r. For example, at the presented MPPT method that is described by the block diagram of Fig. 3, the criterion for no LCO is:

$$\Delta_e = E_{dpi} \times G_{ia} \times \Delta a_{DCO} < \Delta_r \quad ; \quad \begin{cases} E_{dpi} = \dfrac{d(dp_n)}{di_D} \\ G_{ia} = \dfrac{di_D}{dA} \end{cases}, \qquad (7)$$

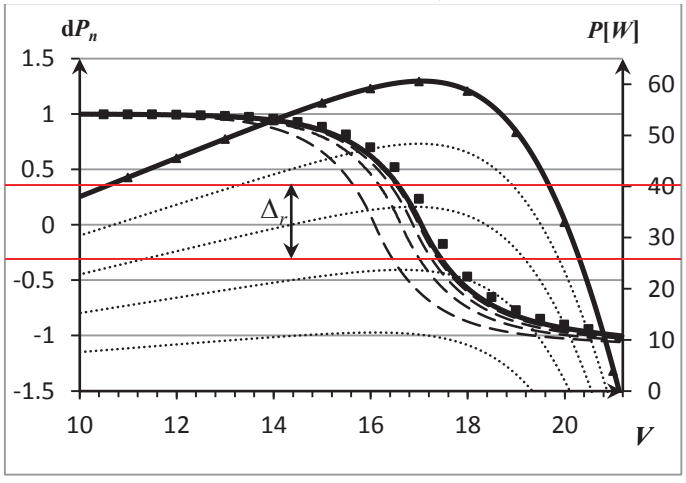

Fig. 1. Typical dp_n and power curves as a function of the panel voltage for various insolation levels.

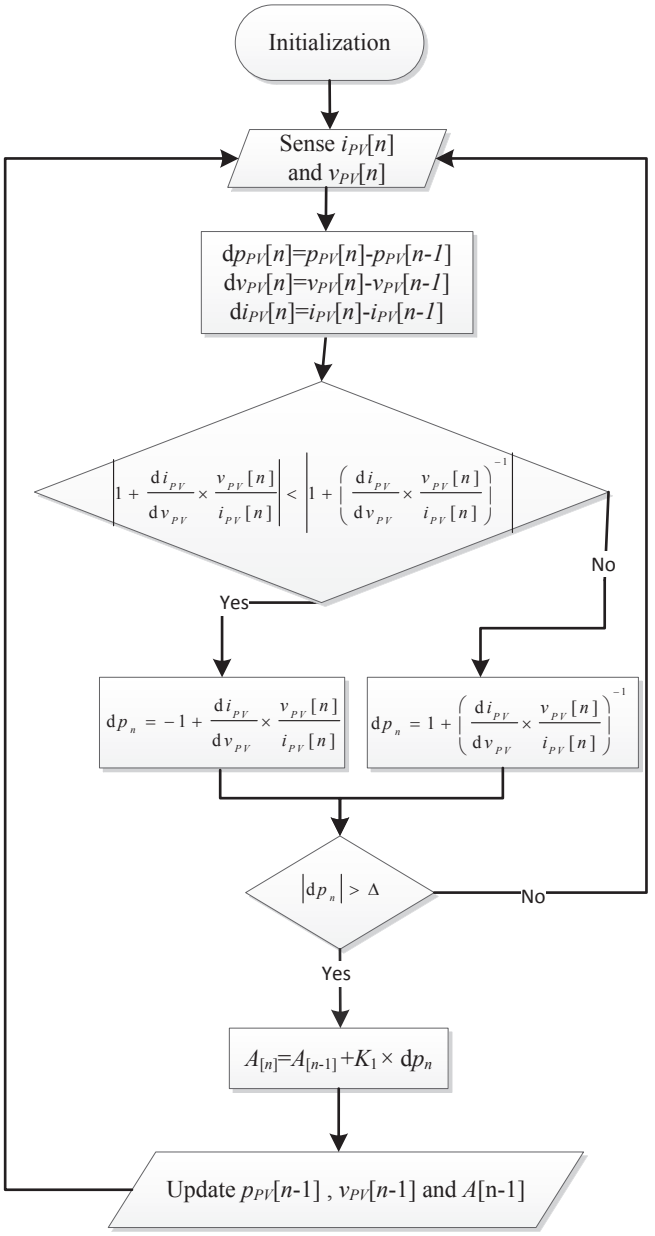

Fig. 2. Flowchart of the modified IncCond MPPT algorithm.

where Δa_{DCO} is the LSB change of DCO control signal $A[n]$, G_{ia} is the small signal transfer function of the converter (control signal to converter output current value) and E_{dpi} is the small signal transfer function of the PVE in its MPP region (input current to error signal).

Since the error signal is not sensed directly, a practical way to eliminate such oscillations is to decrease the resolution of the calculated error around zero by introducing a Zero Error Bin (ZEB) of size Δ_r. The ZEB is defined such that an absolute value of the calculated error less than Δ_r is considered as zero error, indicating the system has converged to its MPP. The size of Δ_r should be set such that the ZEB contains at least one value of measurable error signal (Fig. 1). MPP state unlock condition, is designed by sensing dp_{PV} that exceeds a limitation value defined due to acceptable deviation DC error, Δ_p, from the MPP.

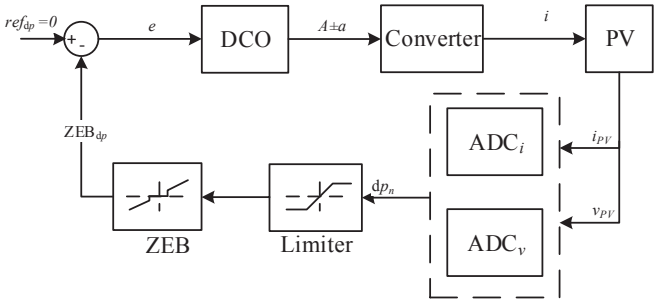

Fig. 3. Block diagram of the control system with Zero Error Bin to avoid LCO

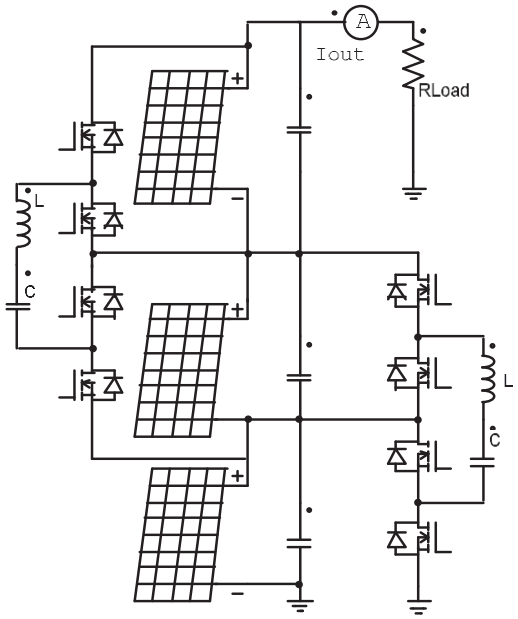

Fig. 4. Three serially connected PVE system with two RSCGC-based DPP

B. *Case study*

To demonstrate the behavior of the LCO, a PSIM (Powersim Inc., ver. 9.0) simulation test bench has been constructed and is shown in Fig. 4, realizing the modified IncCond MPPT algorithm. The algorithm has been applied on a DPP system that comprises three serially connected PVE string [8]. The simulated system consists of a bi-directional converters connected between every two neighboring PVE (Fig. 4). Every DPP is designed to process the necessary amount of power from the neighboring element. The converter that is used to facilitate DPP between two neighboring PVEs is based on a recently published resonant switched-capacitor type voltage controlled current source [8] that features regulation capability without sacrificing the power processing efficiency. In the particular case of this converter, power conversion is governed using pulse density modulation, i.e. frequency control [8].

The results in Fig. 5a show LCO in the control signal, $A[n]$ (the converter's operating frequency) that generates deviations from the MPP as a result of too small Δ_r value. However, in Fig. 5b the Δ_r value satisfies (7), but yet, a DC error can be observed due to the relatively large ZEB (i.e. Δ_p) that has been assigned. Fig. 5c presents a scenario where all of the PVEs are at their MPP by defining Δ_p=0.4W.

IV. Resolution Effects on Power Curve Traps

MPPT algorithms are generally implemented using digital processing, that is by sampling the required signals (using ADC) and generating a correction action. Poor resolution of the measurement may result in power curve traps when estimating the power curve or the instantaneous power derivative as can be observed from Fig. 6 which illustrates possible measurements scenarios for various resolution settings on the sensed current (i_{PVq}) and voltage (v_{PVq}).

Under certain circumstances, power curve traps may exist in the PVE true power curve, or by auxiliary effects [13]. This study examines those which are created due to the ADCs' quantization error. The existence of such traps results in erroneous interpretation of the power derivative, and cause the algorithm to converge into a false MPP point. One possible remedy to this problem can be obtained by averaging the sensed current and voltage, and compensating for any phase lagging due to the moving average implementation. Another more closed-form solution can be realized by estimation the possible deviation from the true (continuous form) error signal. This is done by defining the smallest step size of the control signal, $A[n]$, as follows:

The estimation of the possible deviation from the true error signal in the IncCond MPPT method can be calculated by:

$$Err = (\mathrm{d}p_n) - (\mathrm{d}p_n)_q \; ; \begin{cases} Err_v & ; \; v \le V_{MPP} \\ Err_i & ; \; v > V_{MPP} \end{cases}, \tag{8}$$

where $(\mathrm{d}p_n)_q$ is the calculated $\mathrm{d}p_n$ value, taking into account the quantization effects of the digital platform. The value of Err in the vicinity of the PVEs' MPP can be approximated by [11,12]:

$$\frac{\Delta_i}{\Delta_v} \approx \frac{i_{PV}}{v_{PV}} . \tag{9}$$

Therefore, the expression of Err is:

$$\begin{cases} Err_v = \dfrac{2q_i}{\Delta_v} \times \dfrac{v_1}{i_1}\Big|_{v \approx V_{MPP}} \approx \dfrac{2q_i}{\Delta_i} \\ Err_i = \dfrac{2q_v}{\Delta_i} \times \dfrac{i_1}{v_1}\Big|_{v \approx V_{MPP}} \approx \dfrac{2q_v}{\Delta_v} \end{cases}, \tag{10}$$

where q_i and q_v are the resolution of the current and voltage ADC$_{i/v}$ (potential quantization error).Considering that Err_v and Err_i acquires the greatest value at the MPP. To assure power traps avoidance, the $Err_{v/i}$ has to be carefully appointed. The connection between $q_{i/v}$ and the PVE converter step size can be driven from (10) by appointing a tolerable $Err_{i/v}$.

V. Experimental System and Results

The operation of the modified IncCond MPPT algorithm has been verified on differential power processing architecture using two sets of experiments. One, small-scale experiment, has been constructed to verify in detail the theoretical analysis. The second experiment that has been performed of a full-scale PV string to exemplify a real-world operation. Resonant switched-capacitor type DPP prototypes as in [8] have been used for the experiments with target parameters summarized in TABLE I Current measurement of the PV panel has been facilitated using a sense resistor, serially connected to the controlled PVE.

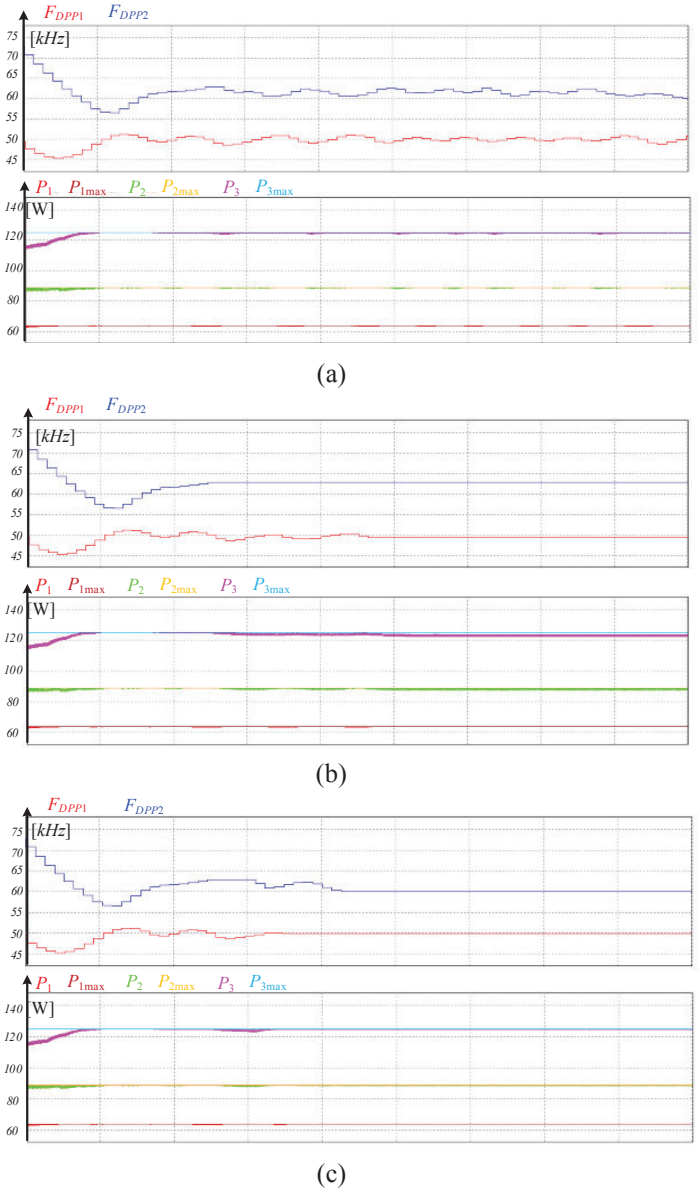

Fig. 5. Simulation results of three PV panels with two DPPs (with $DCO_{Time-Bais}$=1μsec), demonstrating convergence to the MPP. (a) Δ_r =0.00007 (b) Δ_r =0.01 and Δ_p = -1w (c) Δ_r =0.01 and Δ_p = -0.4w.

Both the current and voltage have been sensed using a 10bit ADC of the digital platform. IncCond MPPT algorithm has been implemented digitally on a dsPIC33FJ16GS502 [17]. The value of the error window, Δ_r, has been selected based on the criterion formed in (7) with some error margin due to the tolerance of the practical parameters.

The first experiment has been conducted on a string of three 180W SHARP PV panels (NU-180, E1). The global MPPT of the string has been obtained manually using load adjustments. Two DPP prototypes have been connected to the string to enable local MPPT. Fig. 7 demonstrates the convergence of the lower panel towards MPP. The transient effect is created by switching on the relevant DPP while the second DPP is connected and running, keeping one of the panels at its MPP. TABLE II summarizes the results of several non-uniform shading conditions and presents the harvesting factor , ξ, defined as:

$$\xi = \frac{P_{out}}{\sum_{i=1}^{N} P_{i,MPP}}, \qquad (11)$$

for each experiment, and compares between the operation with and without the DPPs. Fig. 8 shows a picture of the testing environment.

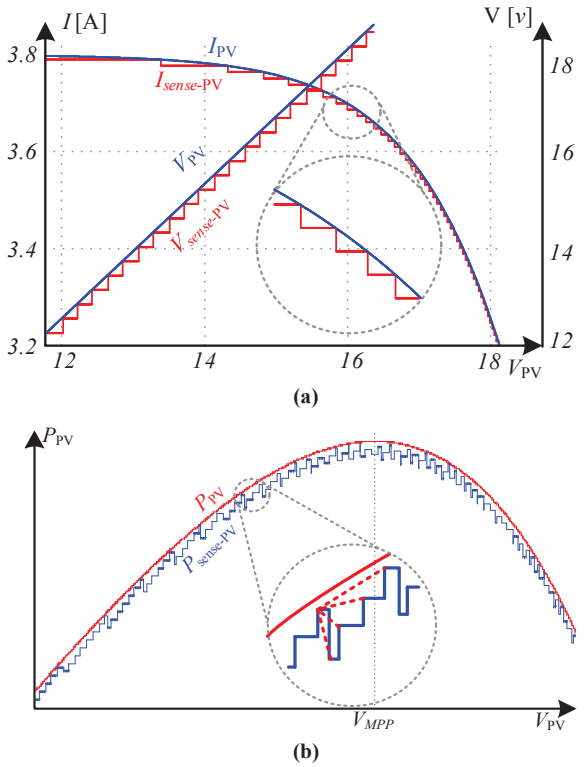

Fig. 6. Resolution effect on power traps in the sensed power curve, where red trace is the true PV element power curve and the blue trace is the sensed power curve.

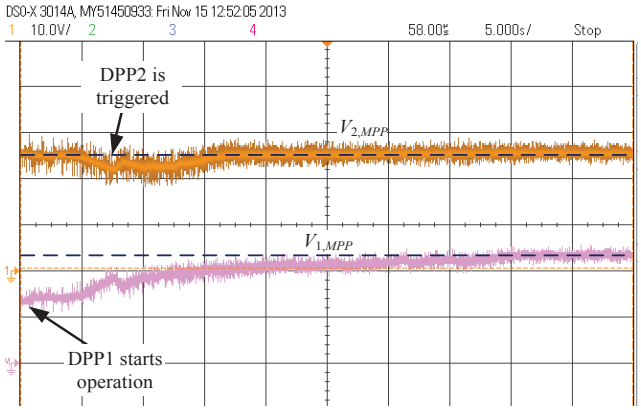

Fig. 7. Experimental results showing convergence to the MPP of the entire string of three panels with two DPPs. Top: voltage of PV1 (10V/div); Bot: voltage of PV2 (10V/div). Horizontal scale: 5sec/div.

TABLE II. HARVEST IMPROVEMENT DUE TO ADDITION OF THE DPPS

$P_{1,MPP}$	$P_{2,MPP}$	$P_{3,MPP}$	P_{ma}	ξ_{diodes}	ξ_{DPP}	Improv
0.5	0.95	1	340	0.78	0.94	21%
0.4	0.95	1	327	0.82	0.9	9.3%
0.42	0.74	1	237	0.68	0.96	42%
0.86	1		233	0.94	0.99	5%
0.65	1		200	0.82	0.97	18%
0.54	1		203	0.81	0.95	17%
0.38	1		193	0.68	0.91	33%

a. Normalized to the power of the strongest panel
b. ξ with central inverter only
c. ξ with DPP and a central inverter

TABLE III. MPP CONDITIONS AND DIFFERENTIAL POWER DEMANDS FOR THE TESTED STRING

	V_{mpp} [V]	I_{mpp} [A]	P_{mpp} [W]	P_{diff} [W]
PV_1	26.7	6.27	167	-20
PV_2	26.7	6.27	167	-40
PV_3	26.7	6.27	167	-59
PV_4	26.7	6.27	167	-79
PV_5	32.3	1.97	64	36
PV_6	26.7	6.27	167	16
PV_7	30.2	4.11	124	59
PV_8	26.7	6.27	167	40
PV_9	26.7	6.27	167	20
PV_{10}	26.7	6.27	167	
Total	26.7	6.27	167	368

Fig. 8. Photograph of the first outdoor experiment. Beer-sheva, Israel. Friday, Nov. 15, 2013.

TABLE I. PROTOTYPE PARAMETERS FOR THE TWO CONDUCTED EXPERIMENTS

	L	C	C_B	Δ_r	MOSFETs	P_{max}	f_{max}	η_{max}
Exp. 1	0.5uH, Ferroxcube	10×0.1uF	5×10uF	0.14	PMOS: IXTP96P085T	150W	130kHz	91%
Exp. 2	RM-8 3F3, n=2, ~1mm	5×0.1uF	10×10uF	0.1	NMOS: IXTP160N10T	120W	200kHz	93%

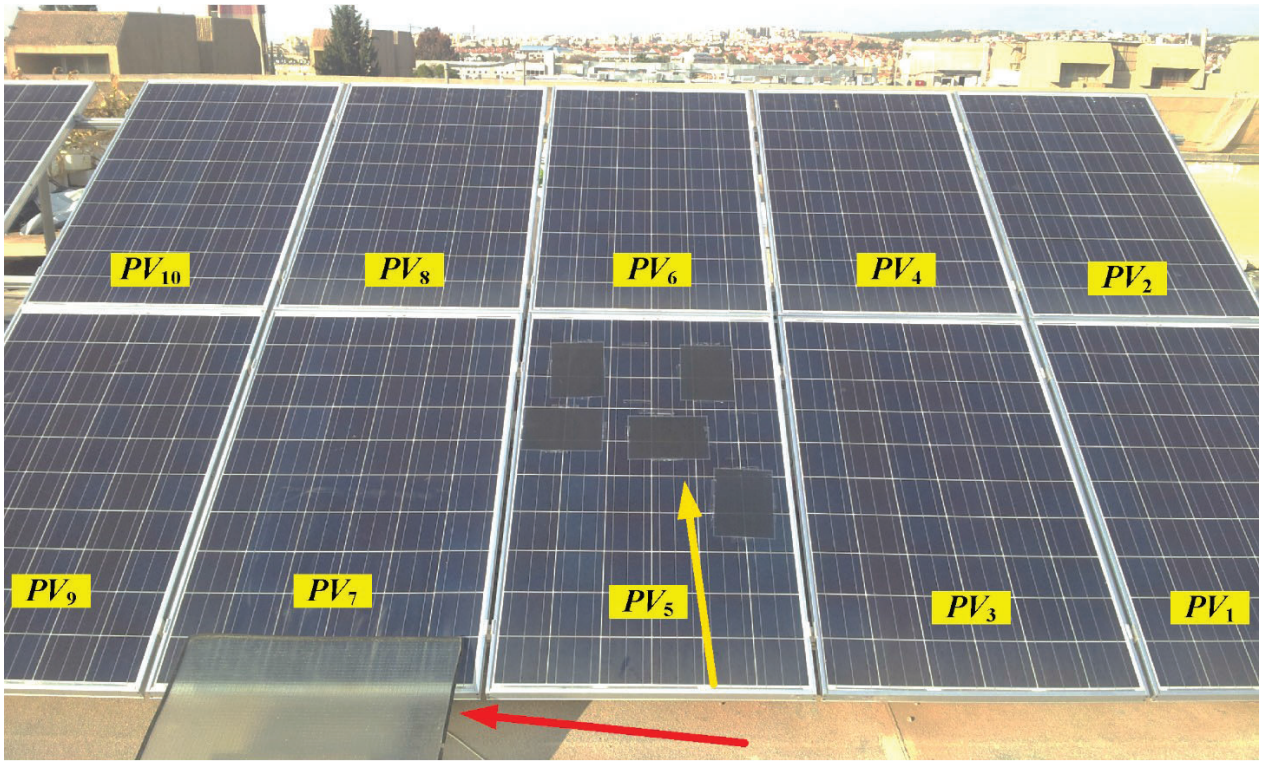

Fig. 9. Photograph of the first outdoor experiment. Beer-sheva, Israel. Sunday, Jan. 16, 2014. PV_5 has five A4-sized filters with opacity of 40%, PV_7 has a diffused glass screen, reducing the irradiation to approximately 75%.

The second experiment has been conducted on a string of ten 245W SHARP PV panels (ND-R245A5) connected to an inverter (ND-R245A5) using nine DPP prototypes. Two panels in the string have been partially shaded as depicted in Fig. 9. A second independent string with the same shading conditions, connected to a second inverter, but without DPP, also examined as a base reference. The test conditions were at an ambient temperature of 16^{O}C and irradiation of approx. 500W/m^2. TABLE III describes each panel's MPP conditions, and the differential power that should be processed to/from the panel. According to TABLE III the differential current that has been processed in few of the DPP units is above 2A. The DPP stabilized on the PVE system absolute MPP in less than a minute from triggering the DPP system with no communication between its RSCGC units.

VI. CONCLUSIONS

A dynamic-gain MPPT algorithm for PV systems was presented and verified. The method has demonstrated a rapid and uniform convergence toward the MPP by employing dynamic steps while owning MPPT control compatibility even for DPPs.

A theoretical analysis on the existence of limit cycle oscillations has been carried out. It revealed that deviation from the MPP can be the result of steady-state oscillations around the MPP due to the finite resolution of the digital hardware, and therefore less energy is extracted. It was also found that the contributors to the oscillations are the frequency/duty-cycle resolution of the DCO and the PVE's converter gain around the MPP, and more importantly that the source, the PV element, also has a dominant factor in the appearance of such oscillations. This is in contrary to other, conventional, switch-mode applications where the source is assumed as constant. The resolution effect on power traps was investigated and their possible deviation error (*Err*) expression was developed, while two conceivable solutions for the discussed power traps were suggested.

The experimental system, using the methods previously discussed, demonstrated dynamic MPP convergence with no LCO realizing significant improvement of power harvesting capability up to 42% for a mini string of only three PV panels (translates into 65W), and 30% for a ten PV string (translates into 300W).

REFERENCES

[1] T. Esram and P. L.Chapman, "Comparison of photovoltaic array maximum power point tracking techniques," *IEEE Trans. Energy Convers.*, vol. 22, no. 2, pp. 439–449, Jun. 2007.

[2] K.A. Kim and P.T. Krein, "Hot spotting and second breakdown effects on reverse I-V characteristics for mono-crystalline Si Photovoltaics," in *Proc. IEEE Appl. Power Electron. Conf. Expo.* , Sept. 2013, pp.1007-1014.

[3] M. Kasper, D.Bortis, and J.W.Kolar, "Classification and Comparative Evaluation of PV Panel-Integrated DC–DC Converter Concepts," *IEEE Trans. Power Electron.* , vol.29, no.5, pp.2511-2526, May 2014.

[4] Y. Nimni and D. Shmilovitz, "A returned energy architecture for improved photovoltaic systems efficiency," in *Proc. IEEE Int. Symp. Circuits and Syst.,* June 2010, pp.2191-2194.

[5] P.S. Shenoy, K.A. Kim, B.B. Johnson, and P.T. Krein, "Differential power processing for increased energy production and reliability of photovoltaic systems," *IEEE Trans. Power Electron.*, vol.28, no.6, pp.2968-2979, June 2013.

[6] S. Ben-Yaakov, A. Blumenfeld, and A. Cervera, "Design and evaluation of a modular resonant switched capacitors equalizer for PV panels," in *Porc. IEEE Energy Conversion Congr. Expo.* , Sept. 2012, pp.4129-4136.

[7] G.R. Walker and J.C. Pierce, "Photovoltaic DC-DC module integrated converter for novel cascaded and bypass grid connection topologies — design and optimisation," in *Proc. IEEE Power Electronics Specialists Conf.*, June 2006, pp.1-7.

[8] A. Blumenfeld, A. Cervera, and M.M. Peretz, "Enhanced Differential Power Processor for PV Systems: Resonant Switched-Capacitor Gyrator Converter with Local MPPT," in *Proc. Appl. Power Electron. Conf. Texas*, Mar.2014 pp.2972-2979.

[9] X. Weidong and W.G. Dunford, "A modified adaptive hill climbing MPPT method for photovoltaic power systems," in *Proc. IEEE 35th Annu. Power Electronics Specialists Conf.*, June 2004, pp.1957-1963.

[10] N. Femia, G. Petrone, G. Spagnuolo, M. Vitelli, "Optimization of perturb and observe maximum power point tracking method," *IEEE Trans. Power Electron.*, vol.20, no.4, pp.963-973, July 2005.

[11] K. H. Hussein and I. Mota, "Maximum photovoltaic power tracking: An algorithm for rapidly changing atmospheric conditions," in *IEE Proc. Generation Transmiss. Distrib*., 1995, pp. 59–64.

[12] L. Fangrui, D. Shanxu, L. Fei L. Bangyin, and K. Yong, "A Variable Step Size INC MPPT Method for PV Systems," *IEEE Trans. Power Electron.* ,vol.55, no.7, pp.2622-2628, July 2008.

[13] D.C. Jones and R.W. Erickson, "Probabilistic Analysis of a Generalized Perturb and Observe Algorithm Featuring Robust Operation in the Presence of Power Curve Traps," *IEEE Trans. Power Electron.*, vol.28, no.6, pp.2912-2926, June 2013.

[14] M.M. Peretz and S. Ben-Yaakov, "Digital control of resonant converters: resolution effects on limit cycles," *IEEE Trans. Power Electron.*, vol.25, no.6, pp.1652-1661, June 2010.

[15] S. R. Sanders, "On limit cycles and describing function method in periodically switched circuits," *IEEE Trans. Circuits Syst.*, vol. 40, no. 9, pp. 564–572, Sep. 1993.

[16] H. Peng, A. Prodic, E. Alarcon, and D. Maksimovic, "Modeling of quantization effects in digitally controlled dc–dc converters," *IEEE Trans. Power Electron.*, vol. 22, no. 1, pp. 208–215, Jan. 2007.

[17] Microchip Technology, Inc., "16-bit digital signal controllers with high-speed PWM, ADC, and comparators," DS70318F, 2012.